Proceedings of IMECE2005
2005 ASME International Mechanical Engineering Congress and Exposition
November 5-11, 2005, Orlando, Florida USA

IMECE2005-82842

DYNAMIC MODEL OF MECHANISMS WITH HIGHLY COMPLIANT MEMBERS

Chao-Chieh Lan
The George W. Woodruff School of Mechanical Engineering, Georgia Institute of Technology
Atlanta, GA 30332 –0405
gtg032j@mail.gatech.edu

Kok-Meng Lee
The George W. Woodruff School of Mechanical Engineering, Georgia Institute of Technology
Atlanta, GA 30332 –0405
kokmeng.lee@me.gatech.edu

ABSTRACT

The dynamic model for links in most mechanisms has often based on small deflection theory without considering geometrical nonlinearity. For applications like light-weight links or high-precision elements, it is necessary to capture the large deflection caused by bending forces. A complete dynamic model is presented here to characterize the motion of a compliant mechanism capable of large deflection with shear and axial deformation. We derive the governing equations from Hamilton's principle along with the essential geometric constraints that relate deformation and coordinate variables, and solve them using a semi-discrete method based on the Newmark scheme and shooting method. The dynamic model has been validated experimentally. We also extend the model for analyzing compliant mechanisms. It is expected that the dynamic model will serve as a basis for analyzing a wide spectrum of compliant multi-link mechanisms.

INTRODUCTION

Dynamic analyses of compliant mechanisms have been a subject of interest for simulation and control of flexible mechanical systems. Examples include space robot arms and high-speed robotic manipulators. These dynamic models are often based on the assumption of linear elasticity without considering geometrical nonlinearity. This assumption is satisfactory provided that the link undergoes a small deflection such that the theory of linear elasticity holds. However, for mechanisms involving highly compliant links (such as rubber fingers in [1], light-weight arms, and high-precision elements), the effects of large deflection on the link motion cannot be ignored. In order to predict more accurately the deflected shape during transient, there is a need to model the dynamics that capture the large deflection compliant link.

In the last two decades, several approaches have been developed to analyze compliant links undergoing large deflection and overall rotation. Javier [2] has divided this research field into three groups. The first is the *simplified elasto-dynamic method* originally proposed by Winfrey [3]. This approach assumes that small deformation does not affect rigid body motion in order to decouple the rigid body motion from the link deformation. The second is the *floating frame formulation* based on defining the deformation relative to a floating frame which follows the rigid body motion of the link. For example, see [4] and [5]. This method makes use of linear finite element (FE) theory since reliable FE packages are widely available. Although this method can account for shear deformation, the deflection is assumed to be small in order for the linear theory of elasticity to hold. The third is the *large rotation vector method* [6~7] based on defining the overall motion plus deformation with respect to the inertial frame. Unlike the floating frame method, this method allows large deflection of compliant link. As a result, nonlinear FE method (FEM) has to be used. This method, when solved using FEM, can lead to excessive shear forces known as shear locking [9] as pointed out by Shabana [8].

We present here a dynamic model based on the generalization of classical beam theory so that it can capture the bending, shear, and axial deformation of a large-deflected compliant mechanism. The classical beam theory was originated by Daniel Bernoulli, which assumes that a straight line transverse to the axis of the beam before deformation remains *straight*, *inextensible*, and *normal to the mid-plane* after deformation. Another important but implicit assumption for classical beam theory is that *the deflection must be small*. Rayleigh [10] latter included the rotatory inertia in the equation of motion. Timoshenko [11] further revealed that the effect of rotatory inertia is small for low frequency vibration but at high frequency the shear stress deformation is comparable to rotatory inertia.

In order to characterize the dynamics of a compliant link, a geometrically exact curvature formula is necessary. The exact

curvature equation that can describe dynamics of a large-deflected link can be found in most calculus textbooks:

$$\frac{d\psi}{ds} = \frac{d^2y/dx^2}{\left[1+(dy/dx)^2\right]^{3/2}} \tag{1}$$

where ψ is the angle of rotation of the link; and s is the arc length from origin to point (x,y) of the link. When the deflection is small, i.e., $dy/dx \ll 1$, (1) reduces to (2).

$$\frac{d\psi}{ds} \approx \frac{d^2y}{dx^2} \tag{2}$$

Equation (1) has been used in several papers to formulate the dynamic equations of a link, such as Reddy *et al.* [12] and Monasa *et al.* [13]. However, as pointed out by Hodges [14], (1) defines the curvature along coordinate x, which is on the original undeflected position of the beam. It does not take into account the well-known shortening effect due to transverse deflections. This resulting error is often unacceptable in many applications when the beam experiences large deflection. In order to overcome this problem, we can parameterize x and y by the arc length s. This leads to another curvature equation;

$$\frac{d\psi}{ds} = \left(x'y'' - x''y'\right) \tag{3}$$

where $x=x(s)$, $y=y(s)$, and the prime denotes derivative with respect to s. Equation (3) has been used by Wagner [15] to derive the dynamics of a large-deflected beam, where the square of (3) is substituted into the strain energy function of the beam in deriving the governing equations based on Hamilton's principle. However, the resulting equations are highly coupled and cannot account for shear deformation of the link.

The difficulty to describe the motion of links undergoing large deflection lies on proper relations between angle of rotation ψ and coordinate variables (x, y). This is because the curvature $d\psi/ds$ is needed to describe the strain energy in addition to the coordinate variables needed to express the kinetic energy. Based on the above observations, we develop a geometrically accurate relation between the angle of rotation and coordinate variables that can be easily incorporated in the dynamic model of large-deflected links. *While the previous angle of rotation is defined without considering shear effect (see (1), (2), and (3)), this paper provides two constraint equations in the derivation of dynamical equations so that angle of rotation induced by bending and shear can both be accommodated.* Built upon our previous model [16] which focuses on the dynamics of a link, in this paper we extend the analysis to general mechanisms with highly compliant members. In addition, the formulation presented here requires no local coordinates.

Specifically, this paper presents a distributed-parameter dynamic model to predict the dynamics of a mechanism with links capable of large deformation, along with a numerical method that uses Newmark algorithm and shooting method in the time and spatial domains respectively. We develop a systematic formulation for analyzing general compliant mechanisms and illustrate this with two application examples.

1 DYNAMIC MODEL OF A COMPLIANT LINK

The dynamic model of complaint link is formulated in two steps. First, we develop two geometric constraint functions to relate the deformation and coordinate variables. Second, we incorporate the constraint equations in the variational form and apply Hamilton's principle to derive the governing equations of the link.

1.1 Geometric constraints

Figure 1 shows a (initially straight) deflected link of length L in the reference frame x-y. In order to fully describe the deflected shape, we define ψ as the initial rotation of the link plus deflection angle induced by bending, and γ as the shear angle. Hence the total angle of rotation is $\psi+\gamma$. Fig. 2(b) shows an infinitesimal segment ds of the link, the coordinate of which can therefore be described by its geometric center (x, y) and the orientation $\psi+\gamma$. We also introduce the axial deformation variable e so that the distance between two adjacent infinitesimal segments is $ds+de$. The variables x, y, γ, ψ, and e are functions of arc length s and time t. They can be expressed explicitly as $x(s,t)$ and $y(s,t)$, etc.

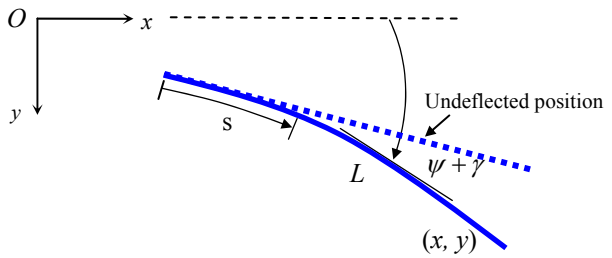

Figure 1 Schematic of a compliant beam

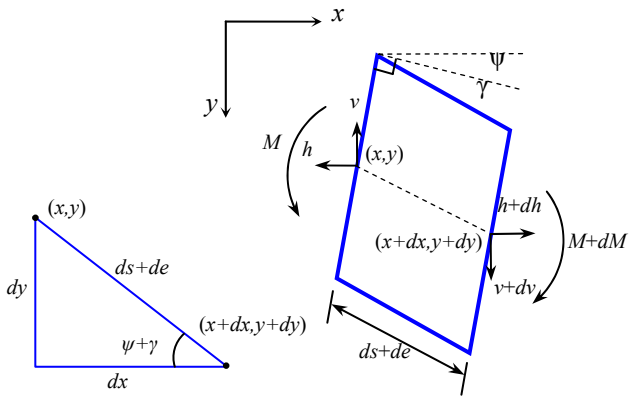

(a) Trigonometric relation (b)Infinitesimal segment

Figure 2 Schematic of an infinitesimal segment

Since the plane motion has only three degrees of freedom, three of the five variables (x, y, ψ, γ, e) are independent. The trigonometry relating the coordinates (x, y) to deformation variables (ψ, γ, e) in the x-y frame can be derived with the aid of Fig. 2(a) and are stated as two geometric constraints:

$$g_1 = x' - (e'+1)\cos(\psi+\gamma) = 0 \tag{4a}$$

$$g_2 = y' - (e'+1)\sin(\psi+\gamma) = 0 \tag{4b}$$

where prime denotes derivative w.r.t. arc length s. Compared with (2) and (3), the shear angle γ and shear deformation e can be embedded in the two geometric constraints in (4) easily. Note that Rao *et al.* [17] have similar constraint equations but again their model cannot capture shear and axial deformation.

At this point, rather than deriving the explicit expressions for ψ and γ from (4), we show in Subsection 1.2 that these two equations can be appended in the variational form by multiplying two Lagrange multipliers (h and v), which result from using more variables (five) than enough (three).

1.2 Formulation using Hamilton's principle

With (4), the equation of motion of the link can be systematically derived using Hamilton's principle, where the following variational form holds:

$$\int_{t_1}^{t_2} \left(\delta K - \delta V + \delta W^{nc} - h\delta g_1 - v\delta g_2\right) dt = 0 \tag{5}$$

where K and V are the kinetic and potential energy of the link respectively; δW^{nc} is the virtual work done by nonconservative forces; and t_1 and t_2 are two arbitrary instant of time. Note that we can append $h\delta g_1$ and $v\delta g_2$ in (5) since g_1 and g_2 are identically zero. With With h and v, we have enough independent variables (five) for the variational procedure.

Following the standard procedure of Hamilton's principle, we first form the total kinetic energy of the link as

$$K = \tfrac{1}{2}\int_0^L \left[I_\rho \dot{\psi}^2 + A_\rho(\dot{x}^2 + \dot{y}^2)\right] ds \tag{6}$$

where I_ρ is moment of inertia of the link; ψ is the angle of rotation induced by bending moment; A_ρ is mass per unit length; and the dot over the variable denotes the time derivative of the variable.

Similarly, the potential (strain) energy of the beam can also be expressed as

$$V = \tfrac{1}{2}\int_0^L \left[EI(\psi')^2 + \kappa GA\gamma^2 + EA(e')^2\right] ds \tag{7}$$

where A is cross-section area and I is the moment of area; E and G are the modulus of elasticity and the modulus of shear respectively; κ is the shear correction factor; γ is the shear angle; and e is the axial elongation. The 1st, 2nd, and 3rd term of (7) represent the strain energy due to bending, shear, and axial deformation respectively.

Equations (6) and (7) express the kinetic and potential energy functions in standard quadratic forms. The nonconservative forces applied at the link include a prescribed rotation ϕ and an external force **F** at the origin O_f. Dissipative forces proportional to the angular velocity can also be accommodated. As an illustration, we use mass proportional damping model to formulate the virtual work as follows:

$$\delta W^{nc} = -\int_0^L \sigma(I_\rho \dot{\psi}\delta\psi + A_\rho \dot{x}\delta x + A_\rho \dot{y}\delta y) ds \tag{8}$$

where σ is the damping coefficient.

The resulting system of partial differential equations that governs the dynamics of the large-deflected link can be obtained using standard manipulations of variational calculus [18]. We further introduce non-dimensional independent variable $u = s/L \in [0,1]$ to replace s so that $x(s,t) = x(u,t)$. The equations can be written as follows after normalization.

$$\frac{EI}{L^2}\psi'' - I_\rho(\ddot{\psi} + \sigma\dot{\psi}) + v\left(\frac{e'}{L} + 1\right)\cos(\psi + \gamma) - h\left(\frac{e'}{L} + 1\right)\sin(\psi + \gamma) = 0 \tag{9a}$$

$$LA_\rho(\ddot{x} + \sigma\dot{x}) - h' = 0\,; \quad LA_\rho(\ddot{y} + \sigma\dot{y}) - v' = 0 \tag{9b,c}$$

$$x' - (L + e')\cos(\psi + \gamma) = 0\,; \; y' - (L + e')\sin(\psi + \gamma) = 0 \tag{9d,e}$$

$$EAe'' - L\left[h\cos(\psi + \gamma) + v\sin(\psi + \gamma)\right]' = 0 \tag{9f}$$

$$\left[v(e' + L)\cos(\psi + \gamma) - h(e' + L)\sin(\psi + \gamma)\right] - L\kappa GA\gamma = 0 \tag{9g}$$

It is clear from (9b,c) that the Lagrange multipliers h and v turn out to be the reaction forces of an infinitesimal segment in the $+x$ and $+y$ direction as shown in Fig. 2(b). The physical interpretations of each equation in (13) are stated as follows.

1. Equation (9a) is the moment balance equation. The rotational inertia in the term is often small, and can be neglected in structural applications. Without deformation, this equation can be reduced to the one that governs rigid-body rotation.
2. Equations (9b,c) are the results of applying Newton's 2nd law to each infinitesimal segment directly.
3. Equations (9d,e) are the normalization of (4). They must be solved simultaneously with the rest of (9).
4. Equation (9f) is the force balance equation in the deformed axial direction. Without the angle of rotation, it reduces to the familiar 2nd order differential equation that governs the axial deformation of a link.
5. Equation (9g) states the shear stress-strain relation where the shear stress comes from the reaction forces h and v.

When the compliant link governed by (9) is subject to a prescribed rotation ϕ at one end and free at the other end, the geometric boundary conditions can be given as follows.

$$\begin{gathered}\psi(0,t) = \phi\,,\, e(0,t) = 0 \\ \text{with } x(0,t) \text{ and } y(0,t) \text{ prescribed}\end{gathered} \tag{10a}$$

From calculus of variation, we can deduce the natural boundary conditions of the link from (12a).

$$\begin{gathered}v(1,t) = 0\,,\, h(1,t) = 0\,,\, \psi'(1,t) = 0 \\ EAe' - \left[h\cos(\psi + \gamma) + v\sin(\psi + \gamma)\right] = 0 \quad \text{at } u{=}1\end{gathered} \tag{10b}$$

Hence we now have enough (eight) boundary conditions in order to solve (9).

2 NUMERICAL APPROXIMATIONS

Equation (9) with the boundary conditions (10) is a system of nonlinear hyperbolic equations with differential constraint equations. We present here a semi-discrete method to solve (9) and (10) numerically. Specifically, the spatial domain u is solved using shooting method while the temporal domain t is solved with Newmark family of integration schemes. For clarity of illustration with limited space, we focus on the model of a free-vibrating link with the following assumptions:

(a) The link is clamped at O with x pointing to the undeflected link direction.

(b) The link is inextensible and has no damping, e=0 and σ=0.

The governing equations of a free-vibrating link then reduce from (9) to (11):

$$\frac{EI}{L^2}\psi'' - I_\rho\ddot{\psi} + \left[v\cos(\psi + \gamma) - h\sin(\psi + \gamma)\right] = 0 \tag{11a}$$

$$LA_\rho\ddot{x} - h' = 0\,; \quad LA_\rho\ddot{y} - v' = 0 \tag{11b,c}$$

$$x' - L\cos(\psi + \gamma) = 0\,; \; y' - L\sin(\psi + \gamma) = 0 \tag{11d,e}$$

$$\left[v\cos(\psi + \gamma) - h\sin(\psi + \gamma)\right] - \kappa GA\gamma = 0 \tag{11f}$$

While developed for a vibrating link, the extension of the numerical scheme to the general mechanisms is rather straightforward.

2.1 Temporal approximation

Motivated by stability considerations, we use the Newmark family of time integration schemes [19] for temporal discretization. Let the position Z_k, its velocity $\dot{Z}_k$, and acceleration $\ddot{Z}_k$ denote the approximate solution to $z(t_k,u)$, $\dot{z}(t_k,u)$, and $\ddot{z}(t_k,u)$ at time level t_k and $u \in [0,1]$ respectively. Assume the solutions of Z_k, $\dot{Z}_k$,

and $\ddot{Z}_k$ have been obtained, the Newmark method is an implicit scheme that finds the approximate solution at next time level t_{k+1} according to the following formulae

$$\ddot{Z}_{k+1} = \frac{2}{a_2(\Delta t)^2}(Z_{k+1} - Z_k) - \frac{2}{a_2 \Delta t}\dot{Z}_k - (\frac{1}{a_2} - 1)\ddot{Z}_k \qquad (12a)$$

$$\dot{Z}_{k+1} = \dot{Z}_k + (1 - a_1)\Delta t \ddot{Z}_k + a_1 \Delta t \ddot{Z}_{k+1} \qquad (12b)$$

where $\Delta t = t_{k+1} - t_k$ denotes the time step size and (a_1, a_2) are Newmark parameters that determine the stability and accuracy of the scheme. By applying (12a), the terms involving time derivatives in (11) can be discretized in the time domain. Following the same convention as above, we use capital letters to represent the approximate solutions, for example, $\Psi_k \approx \psi(t_k, u)$. The discretized differential equations at t_{k+1} can be written as follows.

$$\frac{EI}{L^2}\Psi''_{k+1} - I_\rho\left[\frac{2}{a_2(\Delta t)^2}(\Psi_{k+1} - \Psi_k) - \frac{2}{a_2 \Delta t}\dot{\Psi}_k - (\frac{1}{a_2} - 1)\ddot{\Psi}_k\right] \qquad (13a)$$
$$+ V_{k+1}\cos(\Psi_{k+1} + \Gamma_{k+1}) - H_{k+1}\sin(\Psi_{k+1} + \Gamma_{k+1}) = 0$$

$$LA_\rho\left[\frac{2}{a_2(\Delta t)^2}(X_{k+1} - X_k) - \frac{2}{a_2 \Delta t}\dot{X}_k - (\frac{1}{a_2} - 1)\ddot{X}_k\right] - H'_{k+1} = 0 \qquad (13b)$$

$$LA_\rho\left[\frac{2}{a_2(\Delta t)^2}(Y_{k+1} - Y_k) - \frac{2}{a_2 \Delta t}\dot{Y}_k - (\frac{1}{a_2} - 1)\ddot{Y}_k\right] - V'_{k+1} = 0 \qquad (13c)$$

$$X'_{k+1} = L\cos(\Psi_{k+1} + \Gamma_{k+1});\ Y'_{k+1} = L\sin(\Psi_{k+1} + \Gamma_{k+1}) \qquad (13d,e)$$

$$V_{k+1}\cos(\Psi_{k+1} + \Gamma_{k+1}) - H_{k+1}\sin(\Psi_{k+1} + \Gamma_{k+1}) - \kappa GA\Gamma_{k+1} = 0 \qquad (13f)$$

Equation (13) is a system of time-independent differential and algebraic equations involving unknown functions Ψ_{k+1}, Ψ'_{k+1}, H_{k+1}, V_{k+1}, X_{k+1}, Y_{k+1}, and Γ_{k+1}. The method to solve (13) will be presented in the next section. At the end of time step k+1, the approximate functions $(\dot{\Psi}_{k+1}, \ddot{\Psi}_{k+1})$, $(\dot{X}_{k+1}, \ddot{X}_{k+1})$, and $(\dot{Y}_{k+1}, \ddot{Y}_{k+1})$ will be computed by using (14). Note that the calculation of (13) requires knowledge of the initial conditions $(\Psi_0, \dot{\Psi}_0, \ddot{\Psi}_0)$, $(X_0, \dot{X}_0, \ddot{X}_0)$ and $(Y_0, \dot{Y}_0, \ddot{Y}_0)$. The initial positions and velocities will be given and the initial accelerations can be obtained by assuming zero applied force at t=0 for free vibration of a compliant link.

$$\ddot{\Psi}_0 = \frac{EI}{L^2 I_\rho}\Psi''_0, \quad \ddot{X}_0 = 0, \quad \ddot{Y}_0 = 0 \qquad (14)$$

2.2 Spatial approximation

After temporal discretization, the governing equation reduces to the nonlinear boundary value problem represented by (13). Nonlinear finite element method (NFEM) has often been adopted to solve the BVP numerically. However, the formulation of NFEM is often complicated. In addition, when using FEM to solve problems with shear deformation, there is a numerical problem known as shear locking [9] caused by inadmissible interpolation functions. While several procedures have been made to overcome this problem, we propose in this section an alternative numerical formulation called shooting method that does not suffer from the problem of shear locking.

The basic idea of shooting method is to treat boundary value problems as initial value problems. Consider the following system of n differential equations

$$\mathbf{q}' = \mathbf{f}(u, \mathbf{q}) \qquad (15)$$

where $u \in [0,1]$; $\mathbf{q}_k(0)$ is a $(n\text{-}r)x1$ vector of known initial values; $\mathbf{q}_u(0)$ is a $rx1$ vector of unknown initial values; and $\mathbf{q}_k(1)$ is a $rx1$ vector of known terminal values. In order to integrate (15) as an initial value problem, we have to make r guesses for unknown initial values $\mathbf{q}_u(0)$. The IVP can be integrated numerically using MATLAB ODE solver. After obtaining the trajectories of $\mathbf{q}$, the r given terminal values $\mathbf{q}_k(1)$ have to be matched in order for the solution $\mathbf{q}$ to be true. Hence the procedure is similar to solving r nonlinear algebraic equations except that the explicit forms of the algebraic equations are not known. Iterative procedures used for the shooting method can be found in [20~21].

By setting $\mathbf{q} = [\Psi_{k+1}, \Psi'_{k+1}, H_{k+1}, V_{k+1}, X_{k+1}, Y_{k+1}]^T$, we can recast (13a)~(13e) in the form of a nonlinear ODE coupled with an algebraic equation (13f). The known initial and terminal values of a vibrating link are

$$\mathbf{q}_k(0) = [\Psi_{k+1}(0) \quad X_{k+1}(0) \quad Y_{k+1}(0)]^T = [0 \quad 0 \quad 0]^T$$
$$\mathbf{q}_k(1) = [\Psi'_{k+1}(1) \quad H_{k+1}(1) \quad V_{k+1}(1)]^T = [0 \quad 0 \quad 0]^T \qquad (16)$$

Hence we have to make initial guesses for $\mathbf{q}_u(0)$ to match the given terminal values $\mathbf{q}_k(1)$. The ODE's from (13a)~(13e) can be integrated by Runge-Kutta methods. Note that (13f) is not a differential equation. Hence we cannot incorporate it into the ODE's. However, we still need to know Γ_{k+1} at each R-K step. Since (13f) is true for the entire spatial domain, we can solve it separately at every R-K step j. As shown in (17), the values $V_{k+1,j}$, $H_{k+1,j}$, $\Psi_{k+1,j}$ are known at the j^{th} step.

$$V_{k+1,j}\cos(\Psi_{k+1,j} + \Gamma_{k+1,j}) - H_{k+1,j}\sin(\Psi_{k+1,j} + \Gamma_{k+1,j}) - \kappa GA\Gamma_{k+1,j} = 0 \qquad (17)$$

Hence (17) is a nonlinear equation with one variable $\Gamma_{k+1,j}$. It can be easily solved by bisection method. After obtaining the value of $\Gamma_{k+1,j}$, we can then proceed the next R-K step j+1 from (13) and get the values $V_{k+1,j+1}$, $H_{k+1,j+1}$, $\Psi_{k+1,j+1}$.

In summary, the steps for solving the vibrating link problem are outlined as follows.

Computational Steps:

1. Given (a_1, a_2) with initial conditions $(\Psi_0, \dot{\Psi}_0, \ddot{\Psi}_0)$, $(X_0, \dot{X}_0, \ddot{X}_0)$ and $(Y_0, \dot{Y}_0, \ddot{Y}_0)$,
2. For k=0~# of time steps
   (I) Given initial guesses $\mathbf{q}_u$, solve for $\mathbf{q}$ by an iterative method. At each Runge-Kutta step j, solve (17) to obtain $\Gamma_{k+1,j}$ by bisection method. The value $\Gamma_{k+1,j}$ will be used for the next step j+1.
   (II) After obtaining $\mathbf{q}$, calculate $(\dot{\Psi}_k, \ddot{\Psi}_k)$, $(\dot{X}_k, \ddot{X}_k)$, and $(\dot{Y}_k, \ddot{Y}_k)$ from (12).

End

3 SIMULATIONS AND EXPERIMENT VALIDATION

By using the numerical schemes described in the previous section, we simulate the free vibration of a flexible steel rod whose governing equations are expressed in (11). The simulation parameters are listed in Table 1. The Newmark parameters (a_1, a_2) are (0.5, 0.5), which is known as the constant-average acceleration method and can be proved to be unconditionally stable for any time step. Fig. 3 shows the tip displacement and Fig. 4 shows the snapshots of the vibrating beam, which has a period approximately equal to 0.49 seconds.

Table 1 Simulation parameters and values for a steel rod

Simulation Parameters	Values
Density ρ	7850 kg/m^3
Dimension (LxWxT)	1.11x0.0127x0.0032 m
Young's Modulus E	200GPa
Shear Modulus G	80GPa
(a_1, a_2)	(1/2, 1/2)
Time step size Δt	0.01 sec
Initial tip location	(x,y) = (1.0177m, 0.4061m)
Initial velocity $(\dot{\Psi}_0, \dot{X}_0, \dot{Y}_0)$	(0,0,0)

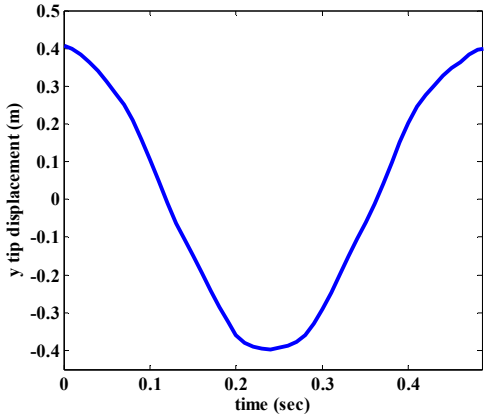

Figure 3 Beam tip displacement in one cycle

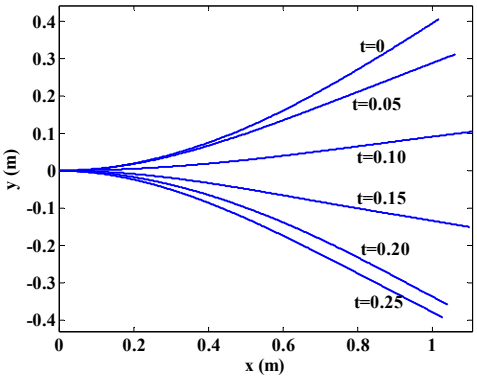

Figure 4 Snapshot of a free-vibrating beam

Figure 5 shows the kinetic energy distribution in one cycle. Clearly, the kinetic energy is dominated by the translational energy in the y direction, which is much larger than the rotational energy. Thus the effect of rotational inertia has always been neglected in structural mechanic problems. Figure 6 shows the energy distribution between kinetic and potential. It is worth noting that there is no energy loss during the temporal integration.

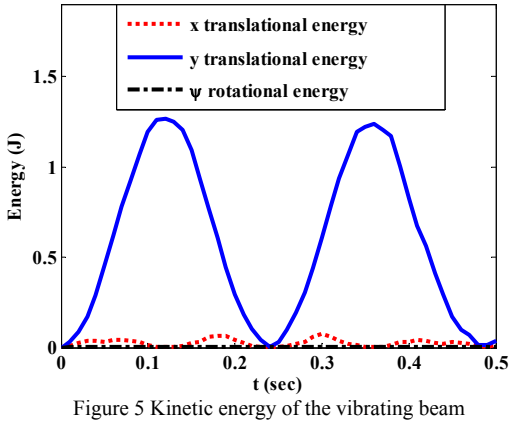

Figure 5 Kinetic energy of the vibrating beam

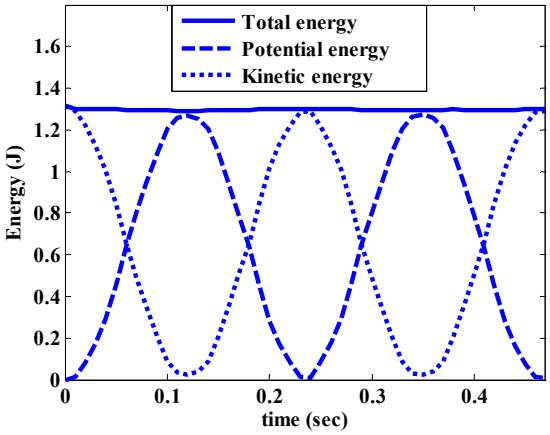

Figure 6 Energy balance of the beam

An experiment has also been conducted to measure the natural frequency of the steel rod whose material properties are listed in Table 1. The x direction of the rod is parallel to the direction of gravity so that the effect of weight is minimized. As shown in Fig. 7, a proximity sensor (Keyence EZ18T) is placed at the undeflected tip position such that it is ON if the tip of the rod approaches and OFF if not. The period of vibration can be recorded by adding two adjacent OFF time intervals. The measured period is approximated 0.485 second which is very close to that predicted by the previous simulation result (0.49 second).

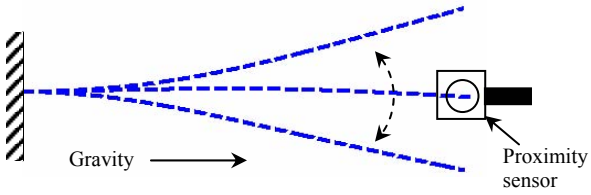

Figure 7 Experiment setup

4 DYNAMIC ANALYSES OF COMPLIANT MECHANISMS

The dynamical model for a compliant link presented in Section 1 can be further extended to analyze mechanisms with compliant members. Since the dynamic model of the link has already based on inertia frame, we can derive the governing equations of links and their associated constraints without introducing intermediate or local frames. We present the dynamic formulation of compliant mechanisms in Subsection 4.1 and illustration examples in Subsection 4.2.

4.1 Formulation of compliant mechanisms

Consider a generic compliant mechanism shown in Fig. 8. The n links are connected in series by n+1 joints where the 0^{th} and $(n+1)^{th}$ joint are ground joints. Each link is governed by six equations from (11). They are rewritten as

$$\frac{E_i I_i}{L_i^2}\psi_i'' + v_i\cos(\psi_i+\gamma_i) - h_i\sin(\psi_i+\gamma_i) = 0 \qquad (18a)$$

$$L_i A_{\rho_i}\ddot{x}_i - h_i' = 0\ ;\quad L_i A_{\rho_i}\ddot{y}_i - v_i' = 0 \qquad (18b,c)$$

$$x_i' - L_i\cos(\psi_i+\gamma_i) = 0\ ;\ y_i' - L_i\sin(\psi_i+\gamma_i) = 0 \qquad (18d,e)$$

$$\left[v_i\cos(\psi_i+\gamma_i) - h_i\sin(\psi_i+\gamma_i)\right] - \kappa_i G_i A_i\gamma_i = 0 \qquad (18f)$$

where the subscript i is w.r.t. the i^{th} link. Note that no intermediate or local frames are required for each link since all of them share the same (inertia) frame x-y. For a mechanism with n links we have $6n$ equations referred to the same inertia

frame. These equations are constrained by the n+1 joints connecting them. Those constraints can be expressed as algebraic equations that must be valid for all time. We list in Table 2 the constraint equations for a joint that connects two links together.

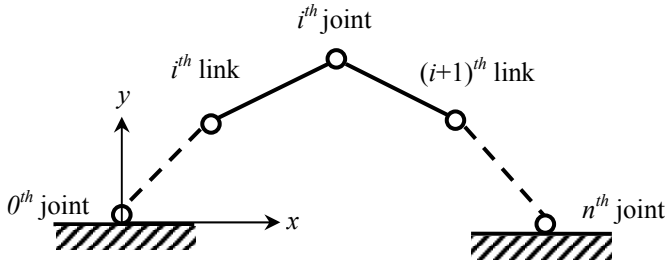

Figure 8 A generic compliant mechanism

Table 2 Constraint equations at the joint

Pinned joint	Clamped joint
$\psi_i'(1)=\psi_{i+1}'(0)=0$	$\psi_i(1)-\psi_{i+1}(0)=$ constant
$h_i(1)+h_{i+1}(0)=0$	$\psi_i'(1)+\psi_{i+1}'(0)=0$
$v_i(1)+v_{i+1}(0)=0$	$h_i(1)+h_{i+1}(0)=0$
$x_i(1)-x_{i+1}(0)=0$	$v_i(1)+v_{i+1}(0)=0$
$y_i(1)-y_{i+1}(0)=0$	$x_i(1)-x_{i+1}(0)=0$
	$y_i(1)-y_{i+1}(0)=0$

For the 0^{th} joint that connects the 1st link to ground, the constraint equations for three types of connections are listed in Table 3. The constraint equations for the n^{th} joint that connects the n^{th} link to ground can be formulated similarly.

Table 3 Constraint equations at the ground link

Fixed	Free	Prismatic
$\begin{cases}\psi_1'(0)=0 & \text{revolute}\\ \psi_1(0)=\text{constant} & \text{clamped}\end{cases}$	$\psi_1'(0)=0$	$\begin{cases}\psi_1'(0)=0 & \text{revolute}\\ \psi_1(0)=\text{constant} & \text{clamped}\end{cases}$
$x_1(0)=0$	$h_1(0)=0$	$h_1(0)=0$ or $v_1(0)=0$
$y_1(0)=0$	$v_1(0)=0$	$x_1(0)=0$ or $y_1(0)=0$

Equation (18) and the constraint equations in Table 2 & 3 form the necessary equations to solve a compliant mechanism. The temporal domain is discretized by Newmark scheme again. In the spatial domain we introduce the Generalized Shooting Method (GSM) [21] to solve the BVP that includes constraint equations as in Table 2 & 3. The basic procedures of GSM are (a) Identify unknown initial values for the BVP (b) Formulate constraint equations that must be satisfied after integrating the BVP as an IVP. The computational steps in Section 2 can be modified slightly to accommodate GSM. We presented in the next subsection two examples that will be solved by GSM in the spatial domain.

4.2 Illustrative examples

Example I illustrates with an open chain mechanism where one link has a prismatic joint. Example II illustrates with a closed chain mechanism with two fixed joints.

Example I A Slider Crank Mechanism

We consider here a slider crank mechanism as shown in Fig. 9. An input torque M drives the mechanism at the base of link 1 that connects link 2 (connecting rod) by joint C. Link 2 is tied to another massless slider block through a revolute joint.

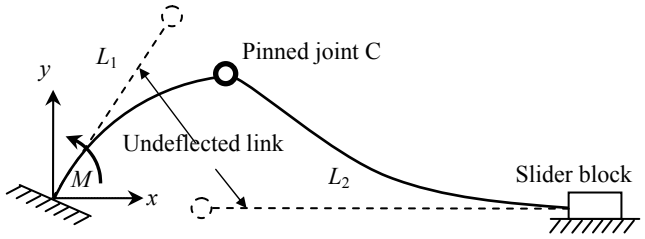

Figure 9 Compliant slider crank mechanism

The input torque at link 1 for different time is given as follows and simulation parameters given in Table 4.

$$M(t)=\begin{cases}0.02t & 0\le t<0.5\\ 0.01 & 0.5\le t<0.7\\ 0.01-0.02(t-0.7) & 0.7\le t<1.2\\ 0 & 1.2\le t\end{cases}$$

Table 4 Simulation parameters and values for the compliant slider crank

Simulation Parameters	Values
Length of link (L_1, L_2)	(0.152, 0.304) m
Density (ρ_1, ρ_2)	(2770, 2770) kg/m^3
Moment of inertia (I_1, I_2)	($4.909\text{x}10^{-10}$, $4.909\text{x}10^{-10}$) m^4
Cross-sectional area (A_1, A_2)	($7.854\text{x}10^{-5}$, $7.854\text{x}10^{-5}$) m^2
Young's Modulus (E_1, E_2)	($1\text{x}10^9$, $5\text{x}10^7$) Pa
(a_1, a_2)	(1/2, 1/2)
Time step size Δt	0.005 sec
Initial tip location	$[x_1(1),y_1(1)]$ = [0.152, 0] m $[x_2(1),y_2(1)]$ = [0.456, 0] m

The displacement of the slider block is shown in Fig. 10 and the midpoint deflection of connecting rod is shown in Fig. 11. We also compare the presented dynamic model with the floating frame formulation (see [4] and [5]) and absolute nodal coordinate formulation [22] in these figures. These results show very good agreement.

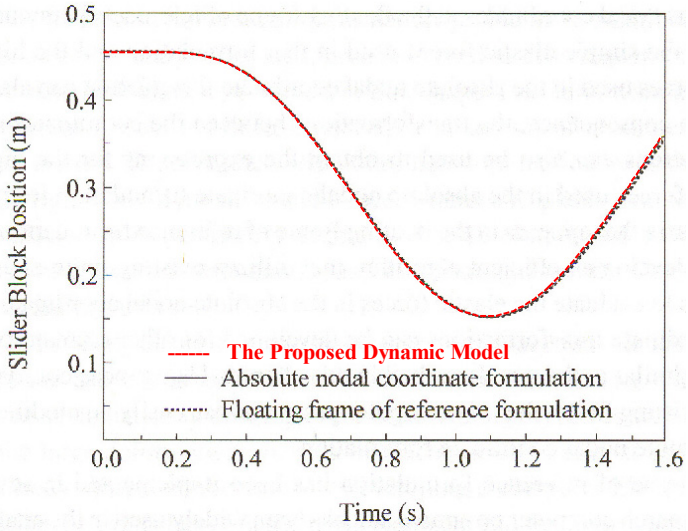

Figure 10 Horizontal position of the slider block

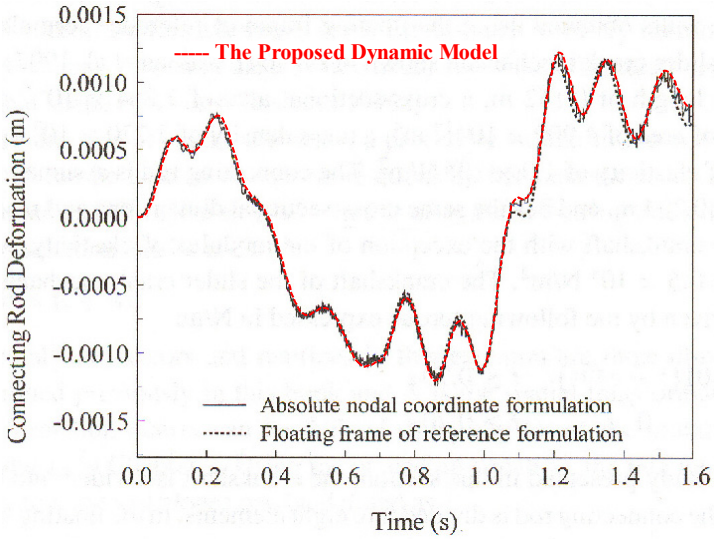

Figure 11 Deformation of link 2

Example II A Four-Bar Mechanism

We study here the dynamics of a compliant closed-chain mechanism with its initial configuration shown in Fig. 12. The coupler (link 2) is made more compliant than the other two links in order to examine the effects of large deformation. Detailed parameters of the mechanism are listed in Table 5.

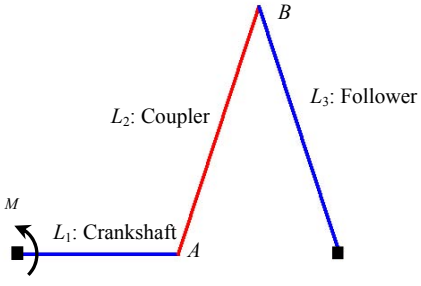

Figure 12 A four-bar mechanism

Table 5 Simulation parameters and values for the compliant slider crank

Parameters	Values
Length of link (L_1, L_2, L_3)	(0.5, 1, 1) m
Density (ρ_1, ρ_2, ρ_3)	(7847, 7847, 7847) kg/m^3
Moment of inertia (I_1, I_2, I_3)	($1.257\text{x}10^{-7}$, $1.257\text{x}10^{-7}$, $1.257\text{x}10^{-7}$) m^4
Cross-sectional area (A_1, A_2, A_3)	($1.257\text{x}10^{-3}$, $1.257\text{x}10^{-3}$, $1.257\text{x}10^{-3}$) m^2
Young's Modulus (E_1, E_2, E_3)	($2.1\text{x}10^{11}$, $2.1\text{x}10^{8}$, $2.1\text{x}10^{11}$) Pa
Initial tip location	$[x_1(0), y_1(0)] = [0, 0]$ m $[x_3(1), y_3(1)] = [1, 0]$ m

The mechanism is initially at rest and the crankshaft is given a moment input from $0 \le t \le 0.6$ as follows.

$$M(t) = \begin{cases} 500t & 0 \le t < 0.2 \\ 100 & 0.2 \le t < 0.4 \\ 100 - 500(t - 0.4) & 0.4 \le t < 0.6 \\ 0 & 0.6 \le t \end{cases}$$

The advantage of the presented energy-based model is that it allows us to easily verify the results by energy balance check. Figure 13 shows the calculated energy which must equal to the applied work apparently. It is obvious that the total kinetic energy is converted to potential energy at t=0.95s. After the potential energy reaches its maximum (and the kinetic energy reaches its minimum), the energy transfers back again to the kinetic component.

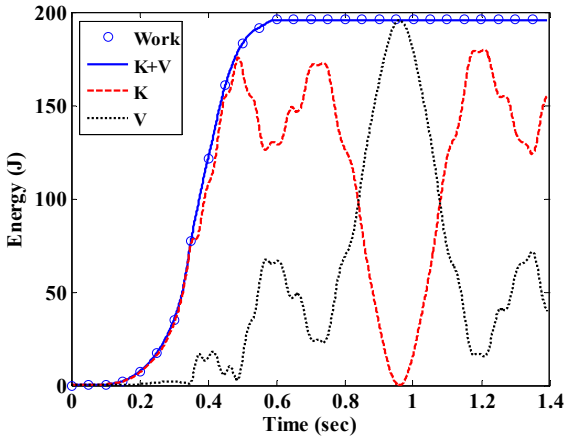

Figure 13 A four-bar mechanism

5 CONCLUSIONS

A complete dynamic model, which accounts for bending, shear and axial deformations with no geometric approximation, has been presented for analyzing compliant links capable of large deflection with large overall motion. Specifically, we showed how the effect of shear angles and axial deformation on large deformation can be incorporated as geometric constraints in the governing equations derived using Hamilton's principle for predicting the transient response of a compliant link. In addition, we demonstrated a numerical method that combines a Newmark scheme with shooting method to solve the equations. An illustrative example of a free-vibrating steel rod has been given to show the application of the model. The simulation result of the vibrating rod has matched well with the experiment data. Finally we develop a systematic formulation to analyze compliant mechanisms. Two illustration examples have been given to verify the formulation.

ACKNOWLEDGMENTS

This project is jointly funded by Georgia Agriculture Technology Research Program and US Poultry and Eggs Association.

REFERENCES

[1] Lee, K.-M., 1999, "On the Development of a Compliant Grasping Mechanism for On-line Handling of Live Objects, Part I: Analytical Model," *Int. Conf. on Advanced Intelligent Mechatronics Proc.* (AIM'99), Atlanta, September 19-23, pp. 354-359.

[2] Javier, G. D. J., Eduardo, B., 1994, *Kinematic and Dynamic* Simulation *of Multibody system*, Spring-Verlag.

[3] Winfrey, R. C., 1971, "*Elastic Link Mechanism Dynamics*," ASME Journal of Engineering for Industry, **93**, pp. 268-272.

[4] Laskin, R. A., Likins, P. W., Longman, R. W., 1983, "*Dynamical Equations of a Free-Free Beam Subject to Large Overall Motions,*" The Journal of the Astronautical Sciences, 31(4), pp.507-528.

[5] Book, W. J., 1984, "*Recursive Lagrangian Dynamics of a* Flexible *Manipulator Arm*," The International Journal of Robotics Research, **3**, pp. 87-101.

[6] Simo, J.C., Vu-Quoc, L., 1986, "*On the dynamics of flexible beams under large overall motions--The plane case: Part I*," ASME Journal of Applied Mechanics, Vol.53, pp.849-854.
[7] Simo, J.C., Vu-Quoc, L., 1986, "*On the dynamics of flexible beams under large overall motions--The plane case: Part II,*" ASME Journal of Applied Mechanics, Vol.53, pp.855-863.
[8] Shabana, A. A., 1998, Dynamics of multibody systems, Wiley, New York.
[9] Bathe, K.-J., 1996, *Finite Element Procedures*, Prentice Hall, N.J.
[10] Rayleigh, J. W. S., 1945, *Theory of Sound*, Vol. 1, Dover, New York.
[11] Timoshenko, S. P., 1922, "*On the Transverse Vibrations of Bars of Uniform Cross-Section*," Philosophical Magazine, **43**, pp.125-131.
[12] Reddy, J. N., Singh, I. R., 1981, "*Large Deflections and Large-Amplitude Free Vibrations of Straight and Curved Beams*," International Journal for Numerical Methods in Engineering, **17**, pp. 829-852.
[13] Monasa, F., Lewis, G., 1983, "*Large Deflections of Point Loaded Cantilevers with Nonlinear Behavior*," Journal of Applied Mathematics and Physics, **34**, pp. 395-402.
[14] Hodges, D. H., 1984, "*Proper Definition of Curvature in Nonlinear Beam Kinematics*," AIAA Journal, **22**, pp.1825-1827.
[15] Wagner, H., 1965, "*Large-amplitude Free Vibrations of a Beam*," Journal of Applied Mechanics, **32**, pp. 887-892.
[16] Lan, C.-C., Lee, K.-M., 2005, "*Dynamic Model of a Compliant Link with Large Deflection and Shear Deformation*," IEEE/ASME Advanced Intelligent Mechatronics, Monterey, CA.
[17] Rao, B. N., Rao, G. V., 1989, "Large Amplitude Vibrations of a Tapered Cantilever Beam," Journal of Sound and Vibration, **127**(1), pp. 173-178.
[18] Weinstock, Robert, 1974, *Calculus of Variations*, Dover Publications Inc., N.Y.
[19] Newmark, N. M., 1959, "*A Method of Computation for Structural Dynamics*," ASCE J. of the Eng. Mechanics division, pp. 67-94.
[20] Rao, B. N., Shastry, B. P., Rao, G. V., 1986, "*Large Deflections of a Cantilever Beam Subjected to a Tip Concentrated Rational Load*," The Aeronautical Journal, **90**, pp. 262-266.
[21] Lan, C.-C., Lee, K.-M., 2005, "*Generalized Shooting Method for Analyzing Compliant Mechanisms*," IEEE International Conference on Robotics and Automation, Barcelona, Spain
[22] Shabana, A. A., 1998, Dynamics of multibody systems, Wiley, New York.